



# The uncertainties and causes of the recent changes in global evapotranspiration from 1982 to 2010

Bo Dong<sup>1</sup> · Aiguo Dai<sup>1,2</sup>

Received: 10 February 2016 / Accepted: 1 September 2016  
© Springer-Verlag Berlin Heidelberg 2016

**Abstract** Recent studies have shown considerable changes in terrestrial evapotranspiration (ET) since the early 1980s, but the causes of these changes remain unclear. In this study, the relative contributions of external climate forcing and internal climate variability to the recent ET changes are examined. Three datasets of global terrestrial ET and the CMIP5 multi-model ensemble mean ET are analyzed, respectively, to quantify the apparent and externally-forced ET changes, while the unforced ET variations are estimated as the apparent ET minus the forced component. Large discrepancies of the ET estimates, in terms of their trend, variability, and temperature- and precipitation-dependence, are found among the three datasets. Results show that the forced global-mean ET exhibits an upward trend of  $0.08 \text{ mm day}^{-1} \text{ century}^{-1}$  from 1982 to 2010. The forced ET also contains considerable multi-year to decadal variations during the latter half of the 20th century that are caused by volcanic aerosols. The spatial patterns and interannual variations of the forced ET are more closely linked to precipitation than temperature. After removing the forced component, the global-mean ET shows a trend ranging from  $-0.07$  to  $0.06 \text{ mm day}^{-1} \text{ century}^{-1}$  during 1982–2010 with varying spatial patterns among the three datasets. Furthermore, linkages between the unforced ET and internal climate modes are examined. Variations in Pacific sea surface

temperatures (SSTs) are found to be consistently correlated with ET over many land areas among the ET datasets. The results suggest that there are large uncertainties in our current estimates of global terrestrial ET for the recent decades, and the greenhouse gas (GHG) and aerosol external forcings account for a large part of the apparent trend in global-mean terrestrial ET since 1982, but Pacific SST and other internal climate variability dominate recent ET variations and changes over most regions.

**Keywords** Evapotranspiration · ET trend · Climate variability · Pacific SST · IPO · CMIP5

## 1 Introduction

Terrestrial evapotranspiration (ET, or land evapotranspiration) is a key component of the global water cycle. It plays a critical role in surface water and energy budgets. Unlike temperature, historical changes in the main components of the water cycle, such as precipitation (Dai et al. 1997; Gu and Adler 2015) and runoff (Dai et al. 2009; Dai 2016), are still dominated by large natural variations. In particular, historical changes in ET remain uncertain. Although many studies indicate an upward trend in global-mean land ET (referred to as “global ET” hereafter) since the 1980s (e.g., Wild et al. 2008; Zeng et al. 2012; Yan et al. 2013), some studies show decreasing global ET over the past few decades (e.g., Seo et al. 2012). Such discrepancy is mainly due to limited long-term ET observations over the globe (Wang and Dickinson 2012). Current long-term global ET estimates are based largely on empirical relationships, water budget analysis, or land surface model simulations; and the results are sensitive to different methods, models and forcing data used.

✉ Aiguo Dai  
adai@albany.edu

<sup>1</sup> Department of Atmospheric and Environmental Sciences,  
University at Albany, State University of New York, Albany,  
NY 12222, USA

<sup>2</sup> National Center for Atmospheric Research (NCAR), Boulder,  
CO, USA

Although the evaporative demand increases along with surface warming (Feng and Fu 2013; Scheff and Frierson 2014; Zhao and Dai 2015), ET over many land areas is constrained by terrestrial water supply. Therefore, changes in precipitation and soil moisture induced by internal climate variability can affect ET. Numerous studies have shown that natural climate variability, such as the El Niño-Southern Oscillation (ENSO), the Pacific Decadal Oscillation (PDO) and the closely related Interdecadal Pacific Oscillation (IPO), and the Atlantic Multi-decadal Oscillation (AMO) (Liu 2012), has large impacts on precipitation over many land areas (e.g., Ropelewski and Halpert 1987, 1989; Mantua et al. 1997; Dai and Wigley 2000; Hu and Feng 2012; Dai 2013; Gu and Adler 2013, 2015; Dong and Dai 2015; García-García and Ummenhofer 2015; Gu et al. 2016). For instance, Dai and Wigley (2000) found that El Niño induces positive precipitation anomalies over East Asia, Pacific coastal South America, the southern and central U.S., but negative anomalies over eastern Australia and the maritime continent, Amazonia, southern Africa, western Canada, and some South Asian monsoon regions. Dong and Dai (2015) found that on decadal to multi-decadal time scales, the warm (cold) phase of the IPO induces considerable decadal precipitation variations over various land regions, such as positive (negative) anomalies over the southwest U.S. and negative (positive) anomalies over southern Africa and eastern Australia. Thus, ENSO, IPO and other natural climate variations can contribute significantly to recent variations and changes in global ET through their influences on precipitation and other climate fields.

Indeed, Jung et al. (2010) showed that the recent slowdown of the global ET upward trend since 1982 coincides with the major El Niño event in 1998, and it results from moisture limitation over Southern Hemisphere land. Yan et al. (2013) suggested that the increases in land precipitation and ET from 1982 to 2011 resulted mainly from prevailing La Niña events since 1999. Miralles et al. (2014) found that ENSO dominates the ET variations during 1980–2011 at the global scale, and attributed the multi-year declines in global ET around 1982, 1991 and 2001 to ENSO's transitions from a cold to a warm phase. All these studies confirm the importance of the tropical Pacific sea surface temperatures (SSTs) in modulating global ET and its apparent trends. Since the IPO (Zhang et al. 1997; Liu 2012) represents the decadal to multi-decadal variations in ENSO activity and its recent transition from a warm to a cold phase around 1999 has caused significant precipitation changes over many land areas (Dai 2013; Dong and Dai 2015), it is natural to expect the IPO to have contributed to the recent ET variations and trends.

In this study, we analyze ET variations and changes since 1982 using three different datasets and climate model simulations, and examined the relationship between the ET

and two of its many controlling factors—temperature (T) and precipitation (P)—to help us identify the nature of the ET trends (i.e., forced vs. unforced). Our main goal is to attribute the ET trends to external climate forcing (such as increased greenhouse gases (GHGs) or volcanic eruptions) or internal climate variations (such as the IPO), rather than to changes in ET's individual drivers. We focus on the ET-T and ET-P relationship partly because reliable long-term data are readily available over most land areas only for these two variables and partly because T and P are the typical climate variables used to represent forced climate responses to external forcing. Therefore, such an analysis can improve our understanding of how ET responds to changes in external forcing. We emphasize that the ET used here includes not only the effects of T and P, but all other ET drivers such as surface solar radiation, wind speed and relative humidity. We use a new approach to isolate the forced (i.e., induced by changes in anthropogenic and natural climate forcings) and unforced (i.e., due to internal climate variability) components of ET, and evaluate the variations and apparent trends in each of them. Differences among the ET datasets are analyzed to reflect the uncertainty in our current estimates of global ET. In addition, tropical Pacific SSTs' influence on global ET is also examined.

We first describe the data and method in Sect. 2. In Sect. 3, we compare the changes and variations in global ET during 1982–2010 based on the three different datasets. Using climate model simulations, the forced component of ET is analyzed in Sect. 4. In Sect. 5, we present an attribution analysis of the recent ET changes to external forcings and natural variability. A summary is given in Sect. 6.

## 2 Data and method

Three different global terrestrial datasets of actual ET (not potential ET) were used in this study. A high-resolution global ET dataset used by Miralles et al. (2014) that was constrained using satellite observations of precipitation, surface soil moisture and vegetation water content was kindly provided by D.G. Miralles (Miralles ET thereafter). This monthly ET dataset covers the period from 1980 to 2011 and is on a  $0.25^\circ \times 0.25^\circ$  global grid. The second ET dataset was from Jung et al. (2010 and updates, Jung ET thereafter), who derived the monthly ET estimates on a  $0.5^\circ \times 0.5^\circ$  global grid from 1982 to 2011 by integrating eddy-covariance ET measurements with surface meteorological data using a machine-learning algorithm (without the use of a land model). The temperature and precipitation forcing data used in the Jung ET were, respectively, from the Climate Research Unit (CRU-TS 3.2.0, Harris et al. 2014) and the Global Precipitation Climatology Center (GPCC V6, Schneider et al. 2008). The third monthly

ET dataset from 1920 to 2010 was from the output of the Community Land Model Version 4.5 (CLM ET thereafter, Oleson et al. 2013). The CLM4.5 was forced with CRU monthly temperature and precipitation plus NCEP/NCAR reanalysis 6-hourly weather variations (Piao et al. 2012) on a 1° global grid. To facilitate the discussions, we refer to these ET data simply as empirical estimates. All the monthly data were annually averaged before any analysis, and all the analyses and global averages are for land areas within 60°S–60°N, except for correlation maps between ET and T or P, for which we showed a domain from 60°S to 75°N. We used the 60°S–60°N domain to focus on IPO's influence from the low latitudes.

The three ET datasets are largely independent of one another because of the large differences in their deriving methods and forcing data. Therefore, comprehensive assessment of the terrestrial ET characteristics can be done by analyzing and comparing these ET estimates, and their differences are taken to represent uncertainty in our current estimates of global ET for the purpose of this study. We examine variations and trends in the ET both regionally and globally. For the trends, a common time period from 1982 to 2010 was selected for all the three ET datasets.

We computed the linear correlation between the ET variations and the associated surface air temperature (T) and precipitation (P) data to quantify the temperature- and precipitation-dependence of ET, even though the ET-T and ET-P relationships may be nonlinear. We recognize that ET is controlled by the availability of surface moisture, which is largely determined by P, and by atmospheric demand for moisture (i.e., potential ET or PET), which is controlled by vegetation, surface temperature, net radiation, wind speed, humidity, and CO<sub>2</sub> concentrations (Dingman 2015). Here, we focus on the ET-T and ET-P relationships because T and P represent the main *climatic controls on ET* (the focus of this study), with P determining the moisture supply for ET and T approximately representing the energy control on ET. The ET-T and ET-P relationships allow us to examine the relative importance of the energy and water limitations on ET in the different ET products, which may help evaluate the reliability of the ET datasets. Furthermore, because T and P are often used to quantify climate changes associated with GHG increases or changes in oceanic conditions associated with internal climate modes such as the IPO (Dong and Dai 2015), such an analysis can also help us identify the nature of the ET trends (i.e., due to external forcing or unforced internal climate variability).

We examined the ET-T and ET-P relationships with and without trends in the data (by linearly removing the least square fit) in order to separate the contributions of the trends and interannual to decadal variations to their correlations. For the Miralles ET, the original T and P data were combinations of a series of satellite observations

and reanalysis data, which were unavailable to this study. Instead, we used the Climate Prediction Center (CPC) CMAP precipitation (Xie and Arkin 1997) and ERA interim temperature as surrogates because they are partly used as their original forcing data. We also correlated the Miralles ET with the T and P data that were used for the other two ET datasets. As expected, the results are insensitive to the choice of the T and P data.

We used the ensemble mean ET from 59 all-forcing historical simulations from 33 models participated in the Climate Model Inter-comparison Project Phase 5 (CMIP5, Taylor et al. 2012; CMIP5 ET thereafter) to derive the forced component of ET induced by historical changes in anthropogenic (mainly GHGs and sulfate and black carbon aerosols) and natural (volcanic aerosols and solar irradiance changes) forcings. Some of the spatial and temporal characteristics of the forced ET and its associated T or P patterns were estimated using a Maximum Covariance Analysis (MCA) (Bretherton et al. 1992) of the ET together with T or P. The MCA is a useful tool for finding the leading modes in the covariance matrix of two physically-related fields (e.g., T and ET, or P and ET). We then compared the principal components (PCs) of the leading MCA modes to the time series of the historical anthropogenic and natural radiative forcing taken from Fig. 8.18 of Myhre et al. (2013) to attribute the ET modes to the individual forcing agents, aided by the well-known spatial patterns of the forced T change (Collins et al. 2013). We emphasize that it is impossible to estimate the forced ET component directly from the empirical ET datasets using a statistical method due to the relatively short length of record and the mixing of the relatively weak signal of forced changes with large unforced variations, some of which are correlated with the forced changes. Here, we take advantage of the CMIP5 multi-model ensemble mean ET, which was designed to represent the long-term forced changes but not the unforced variations that have occurred in the real world.

To estimate the unforced ET component, we first performed an empirical orthogonal function (EOF) analysis (Monahan et al. 2009) of the CMIP5 multi-model ensemble mean ET from 1920 to 2010 on a global domain of 60°S–60°N and found that the first two leading EOFs account for almost all the forced components of the ET as represented by the CMIP5 multi-model ensemble mean, including those large and brief drops of ET caused by volcanic eruptions in 1963 (Mount Agung), 1982 (El Chichón) and 1991 (Pinatubo) (Angell 1993). We then reconstructed the ET represented by the two EOFs, and then multiplied this ET by a scaling factor  $f$  at each grid point to represent the forced component in the ET datasets. The scaling factor was used to account for the systematic mean biases between the model ET and the empirical ET from each of

the datasets. This factor is defined as  $f = \overline{ET_{obs}} / \overline{ET_{CMIP5}}$ , where the  $\overline{ET_{obs}}$  and  $\overline{ET_{CMIP5}}$  are the long-term (1982–2010) mean ET at each grid point from one of the ET datasets and the CMIP5 models, respectively. To validate the forced ET estimated from the EOF analysis, we performed an MCA of the CMIP5 ensemble mean ET together with each of the three ET datasets separately for the period from 1982 to 2010 on a global domain of 60°S–60°N. The purpose of this MCA was to extract the ET component from each of the three ET estimates that are associated with the spatial and temporal structures of the forced ET seen in the CMIP5 models. For the CLM ET, we also did the same MCA for a longer period from 1920 to 2010. The estimated forced ET components for 1982–2010 from these two MCA analyses for the CLM ET are similar, which suggests that our estimates of the forced ET based on the data from 1982 to 2010 only are likely reliable. This is important as the other two ET datasets do not have data before 1982.

The estimates of the forced ET component from the two methods are comparable. The unforced ET component was subsequently obtained by subtracting the forced ET (based on the EOF method) from the original ET datasets at each grid point. One caveat of this method is that the uncertainties and errors in the CMIP5 ET will propagate into the estimated unforced ET, thus affecting the reliability of the estimated unforced ET, although the bias-corrected CMIP5 multi-model ensemble mean ET likely represents our best estimate of externally forced ET changes. Linear trends were then computed for the forced and unforced ET components. Based on Jung et al. (2010), Miralles et al. (2014) and other studies (see Sect. 1), we hypothesize that the unforced Pacific SST variability accounts for a large part of the unforced ET variability including decadal variations and trends over many land areas. To test it, we first compared the linear trend and variations in the unforced ET with a SST index associated with the IPO. In addition, to physically link regional ET to tropical Pacific SSTs, we also examined the co-variations of regional T and P with tropical Pacific SSTs, together with the ET-T and ET-P relationship. Since T and P are two of the key drivers for ET, the Pacific SST-induced T and P variations can cause ET changes over the same regions.

By assigning the original grid values to finer grid boxes (e.g., 0.1°) and then averaging these fine-grid values over new target grid boxes, we re-mapped all the ET, T, and P data from the observations, empirical estimates and CMIP5 models onto a common  $2.5^\circ \times 2.5^\circ$  grid before any averaging and analyses. Since our focus is on multi-year to decadal variations and long-term changes, we analyzed annual-mean values only. We realize that some of the annual precipitation during a calendar year may stay on the ground or in the soil layer and contribute to ET of the next year, thereby leading to a stronger correlation with a lag between

P and ET. The length of such a lag and its effect likely vary spatially. Here we did not explore this complex lag between P and ET since our focus is on long-term relationships.

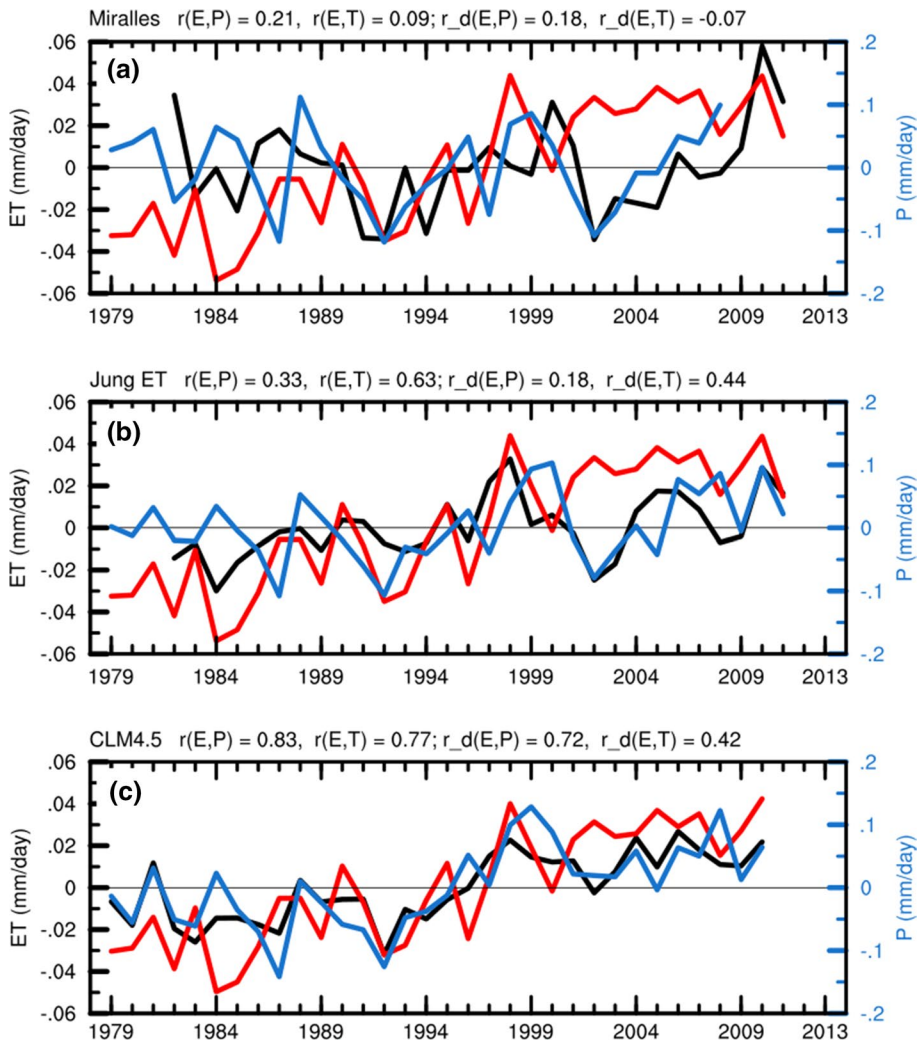
### 3 Changes and variations in ET from 1982 to 2010

Global (60°S–60°N) averaged annual ET and its associated T and P (considered as forcing of ET) for the three ET datasets are shown in Fig. 1. The correlation between the ET time series is 0.33 for Miralles and Jung, 0.66 for Jung and CLM, and 0.31 for Miralles and CLM. The global-mean ET trend for 1982–2010 is 0.01 (statistically insignificant), 0.09, and 0.14 mm/day/century for the Miralles, Jung and CLM datasets, respectively. These results suggest that there exists large disagreement in both the trend and interannual variations among these global ET estimates. The relatively higher correlation between Jung and CLM ET is partially because that they used the same CRU TS 3.20 temperature data. Correlations of the Global-mean ET with the P and T forcing data are strong [ $r(ET, T) = 0.77$  and  $r(ET, P) = 0.83$ ] for the CLM dataset, but are relatively weak for the other datasets, except the Jung ET and T ( $r = 0.63$ , Fig. 1). The correlations weaken when the trends are removed from these time series. This suggests that there exist some concurring trends in the ET and its forcing data that enhance their correlations. This is especially true for CLM ET, with its upward trend correlated with the upward trends in P and T (Fig. 1c).

Spatial patterns of the annual ET trends for the three datasets are shown in Fig. 2, which shows general agreement in the sign of change over Eurasia (mostly increases), southern Africa (increases), the southwest U.S. (decreases), and central South America (decreases). However, the magnitudes of the change differ among them, with the Miralles ET having larger trends than the other two datasets over most of the regions. When averaged over the globe, the Miralles ET trend is very small and insignificant as a result of cancellation between strong positive and negative trend patterns. Large trend discrepancies are seen over the Amazonia, Sahel, eastern and central Africa, and Australia among the three datasets (Fig. 2).

The discrepancies among these ET datasets result in part from the different forcing data and algorithms used to derive the ET estimates. Spatial distributions of the non-detrended annual ET vs. T and ET vs. P correlation are shown in Figs. 3 and 4, respectively. As expected, ET is negatively correlated with T, but positively correlated with P over many dry lands, such as Australia, southern Africa, the western U.S. and Mexico, the Middle East and central and western Asia. Over these dry lands, ET is often limited by availability of soil moisture (Dingman 2015), which increases with precipitation. Surface T often increases as

**Fig. 1** Global ( $60^{\circ}\text{S}$ – $60^{\circ}\text{N}$ ) averaged time series of land evapotranspiration (ET, black curve) and the associated precipitation (P, blue curve) and surface air temperature (T, red curve, the scale is 10 times the ET axis value, in units of  $^{\circ}\text{C}$ ) forcing for the **a** Miralles, **b** Jung and **c** CLM dataset. The correlation coefficients between each pair of time series are indicated as  $r$  values on top of each panel. The  $r_d$  values are for the correlation of detrended time series. The correlation between the three ET series is 0.33 for Miralles vs. Jung, 0.66 for Jung vs. CLM, and 0.31 for Miralles vs. CLM. The ET linear trend from 1982 to 2010 is 0.01, 0.09, and  $0.14 \text{ mm day}^{-1} \text{ century}^{-1}$  for the Miralles, Jung and CLM data sets, respectively

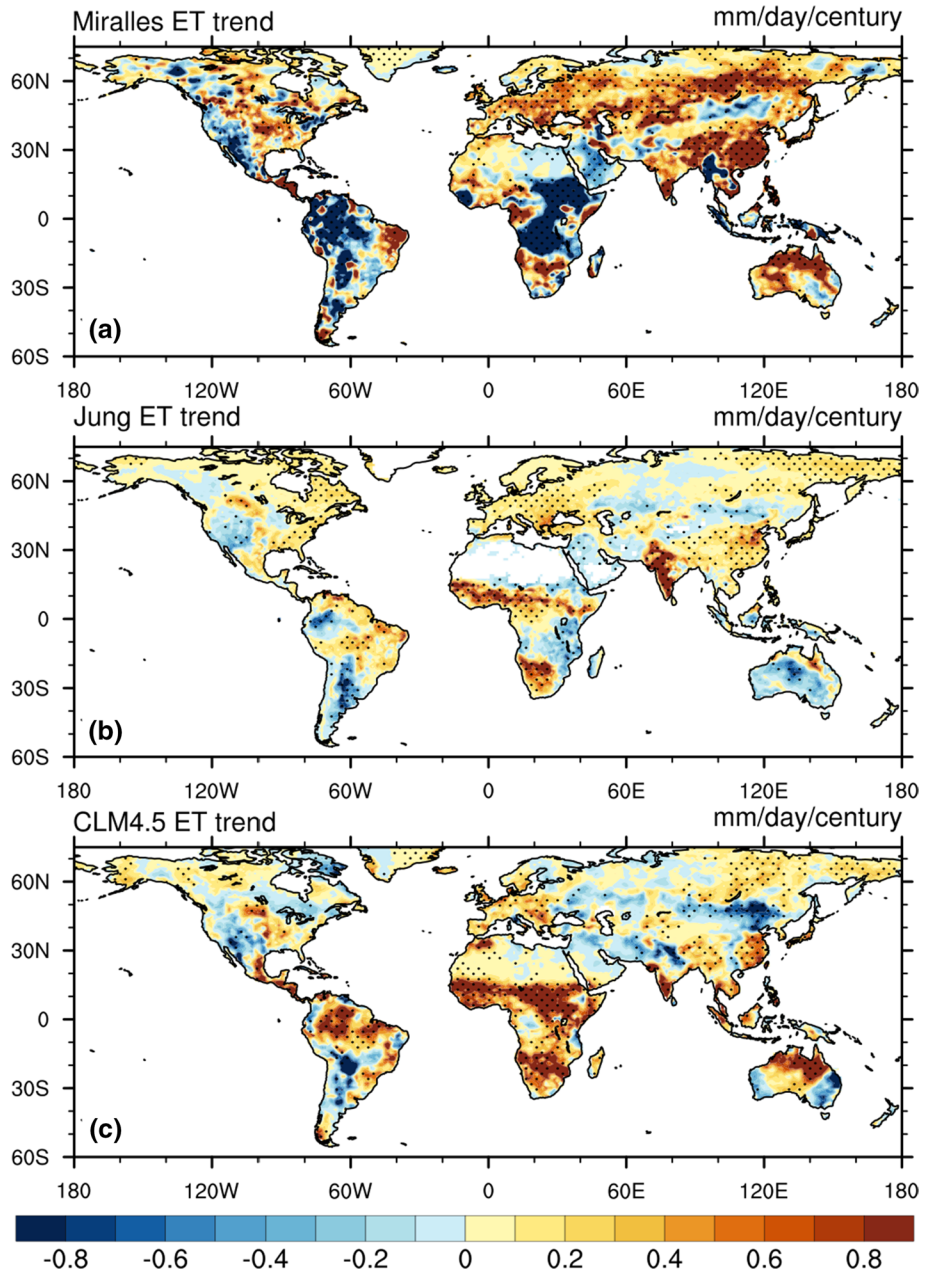


ET declines because most solar heating is used to raise surface T over these regions. Over many other regions, however, there is no consensus on the sensitivity of ET to P and T among these datasets. The Jung ET shows stronger correlations with T than the other two datasets, especially over the northern mid- to high-latitudes; while the CLM ET and, to a lesser degree, Miralles ET are more closely coupled with precipitation (Figs. 3, 4). Correlations based on detrended data exhibit similar spatial pattern with slightly reduced magnitude (not shown), which implies that interannual to multi-year variations contribute most to the total correlation. These results are consistent with the correlations between the global-mean ET and their T and P forcings shown in Fig. 1.

Among the three ET datasets, only the CLM ET covers the whole 20th century. Figure 5 shows the long-term CLM ET trend for 1920–2010, when tropical SSTs have sufficient observations. The long-term trend exhibits reduced magnitudes and different patterns compared to those for 1982–2010 shown in Figs. 1c and 2c. For example, over the

Sahel and most of the U.S., the ET trend shows opposite signs for the two periods. In addition, the global-mean ET trend is  $0.02 \text{ mm/day/century}$  for 1920–2010, much smaller than  $0.14 \text{ mm/day/century}$  for 1982–2010. Figure 5b shows considerable multi-decadal variations in the CLM global-mean ET, with the upward movement since the 1990s contributing the most to the trend for the whole 1920–2010 period. These multi-decadal variations are significantly correlated (with the effective degree of freedom with serial correlation being accounted for in the statistical significance test) with the smoothed IPO index ( $r = -0.40$ ), especially since the 1970s (Fig. 5b). In particular, Fig. 5b suggests that the apparent ET upward trend since the late 1980s is associated with the IPO phase change during this period. This is physically possible as the IPO has significant influences on T and P over many land areas (Dai 2013; Dong and Dai 2015). Even with this physical linkage, however, a close association between the IPO and ET trends since the 1970s does not necessarily imply that the recent IPO phase change is the primary contributor to the recent

**Fig. 2** Linear trends in annual ET from 1982 to 2010 for the **a** Miralles, **b** Jung and **c** CLM4.5 ET dataset. Trends that are statistical significant at the 10 % level are stippled



ET increase. As we show below, about half of the CLM ET trend for 1982–2010 is likely due to GHG and other external forcing, leaving about half of it for the IPO and other internal climate variability.

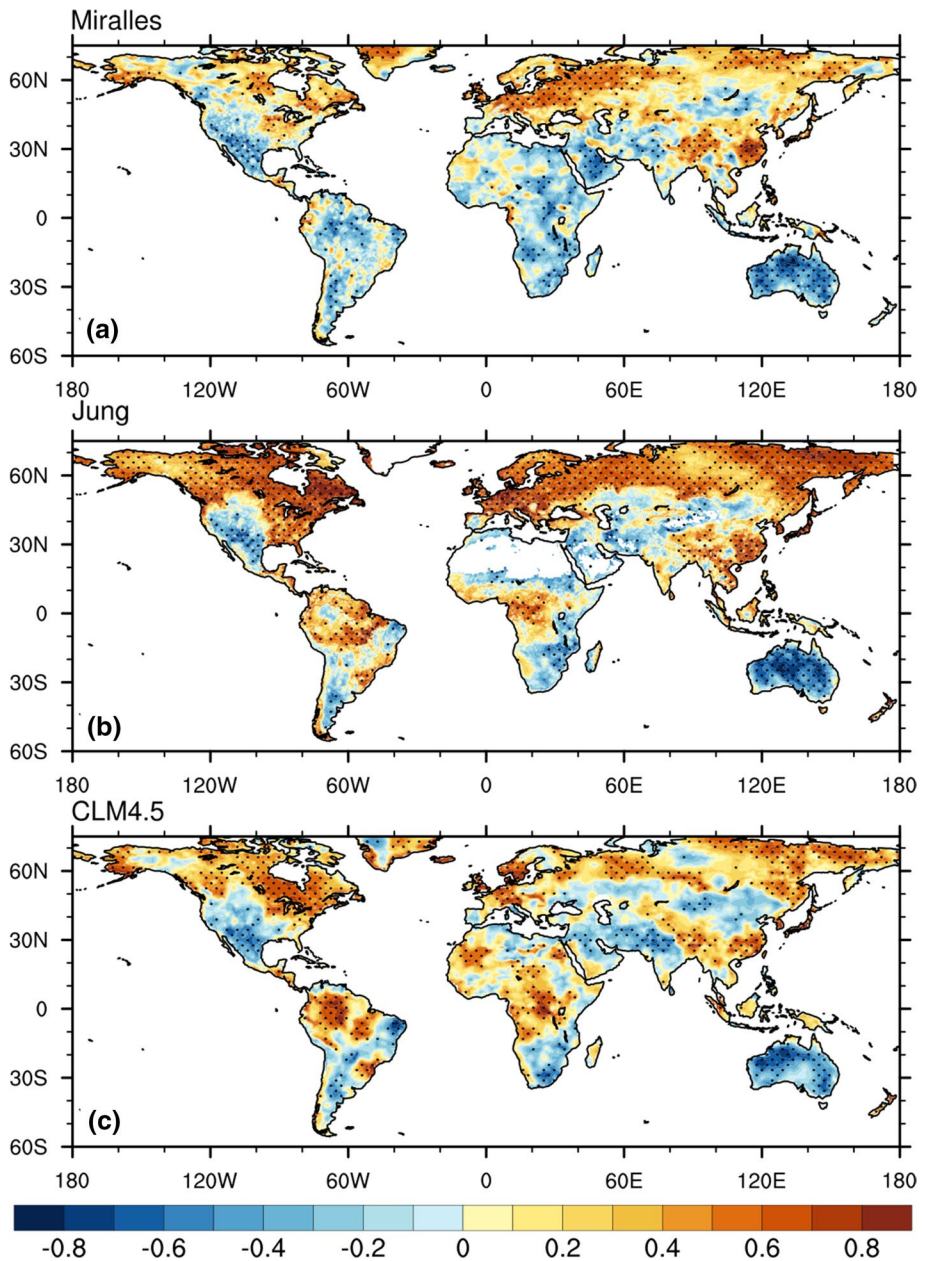
#### 4 Responses of ET to historical forcings in CMIP5 models

Since we use the CMIP5 model-simulated ET to estimate the forced ET component during recent decades, here we describe the characteristics of this ET component and its associated T and P change patterns. We first describe the

EOF decomposition results and then the results from MCA analyses.

Figure 6 shows the two leading EOFs and the associated PCs of the CMIP5 multi-model ensemble-mean ET from 1920–2010 from the all-forcing historical simulations (Taylor et al. 2012). The first (second) EOF explains 36.6 % (16.2 %) of the total variance. The PC1 shows an upward trend that is highly correlated ( $r = 0.92$ ) with the anthropogenic forcing series, while the PC2 shows multi-year and decadal variations associated with the natural forcing ( $r = 0.66$ ) except for the last 12 years, during which the PC2 may be contaminated by the trend represented by the PC1 (Fig. 6b, d). The EOF1 (Fig. 6a, b) shows increasing

**Fig. 3** Maps of the correlation between annual T and ET for **a** Miralles, **b** Jung and **c** CLM4.5 dataset from 1982 to 2010. Stippling indicates the correlation is statistical significant at the 10 % level

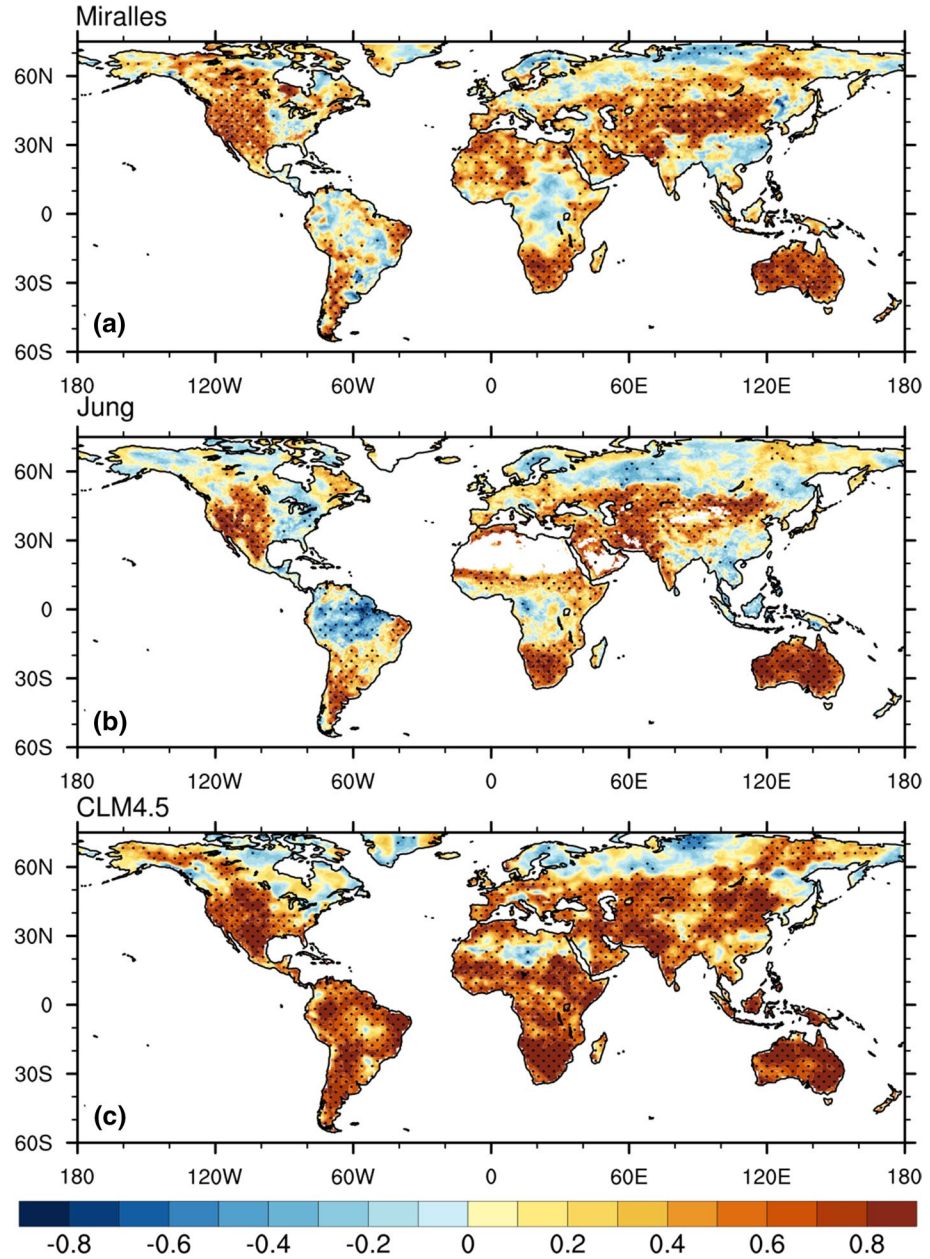


ET over Australia and most Eurasia and North America but decreasing ET over most Africa, northern South America, Southwest North America, and Southeast Asia; whereas the EOF2 shows large declines of ET over most land areas during a period of a few years following volcanic eruptions in 1963 (Agung), 1982 (El Chichón) and 1991 (Pinatubo; Fig. 6c, d). Such large ET anomalies may even affect the ET trend on decadal time scales (e.g., Fig. 5b). Both the EOF patterns and the PC time series are comparable to those derived from the MCA analyses shown in Figs. 7 and 8. The ET decreases shown in Fig. 6a result primarily from decreased precipitation over East and South Asia (likely due to anthropogenic aerosols) and the low latitude Americas,

southern Africa and the Mediterranean region (likely due to GHGs, see Myhre et al. 2013). The spatial coefficients of EOF1 (Fig. 6a) have a global mean ( $60^{\circ}\text{S}$ – $60^{\circ}\text{N}$ ) close to zero due to cancellation between the positive and negative values. Because of this, the EOF1 mode does not result in significant trends in global-mean ET, even though it represents long-term trends over many regions. Instead, the global-mean ET trend in the model ensemble mean ET is attributed mostly to the EOF2, which represents a significant global-mean ET trend of  $0.08 \text{ mm day}^{-1} \text{ century}^{-1}$  from 1982 to 2010.

Together, the EOF1 and EOF2 explain about 52.8 % of the total variance in the ensemble-mean ET field. As

**Fig. 4** Same as Fig. 3 but for correlation between annual P and ET



explained further below, we consider the EOF1 (EOF2) as the response primarily to the anthropogenic (natural) forcing because of the temporal match between the PCs and the forcing series (except the period since the late 1990s as noted above) and the associated spatial patterns of T that match the known T response to GHG forcing, as shown below. Higher-order EOFs of the ensemble-mean ET are mostly high-frequency noises that contribute to the total variance but little to the trends or decadal variations. Thus, using the full ensemble-mean ET field or its EOF1 + EOF2 to remove the forced components in the observations yielded similar results. Here we only show the case based on the EOF1 (due to

anthropogenic forcing) plus EOF2 (due to natural forcing) reconstruction.

Another way to extract the forced ET and its associated T and P patterns in the CMIP5 models is through MCA analyses. The coupled spatial and temporal patterns in the CMIP5 model ET and P or T, as represented by the two leading MCA modes, denoted as MCA(T, E) and MCA(P, E), are shown in Figs. 7 and 8. The spatial patterns and time series of the ET first mode with T and P, denoted as MCA1(T, E) and MCA1(P, E), are similar, which explain 36.5 and 51.0 % of the total ET variance, respectively; thus only that from the MCA1(P, E) case is shown in Fig. 7. The PCs for the MCA1 represent an upward trend that is highly

**Fig. 5** **a** Map of the linear trend in the annual ET from the CLM data set for 1920–2010, and **b** its global ( $60^{\circ}\text{S}$ – $60^{\circ}\text{N}$ ) averaged time series, in which the dashed black line is a 3-year moving average of the annual ET series, and the solid black line is a further smoothed ET series derived using 9-year moving averaging twice of the dashed black line. The dashed blue line is the 2nd principal component of Pacific SSTs from Dong and Dai (2015), namely the Pacific Variability Index (PVI). The solid blue line is the IPO index, which is similarly smoothed based on the dashed blue line. The correlation between the dashed (solid) black and blue lines is  $-0.29$  ( $-0.40$ )

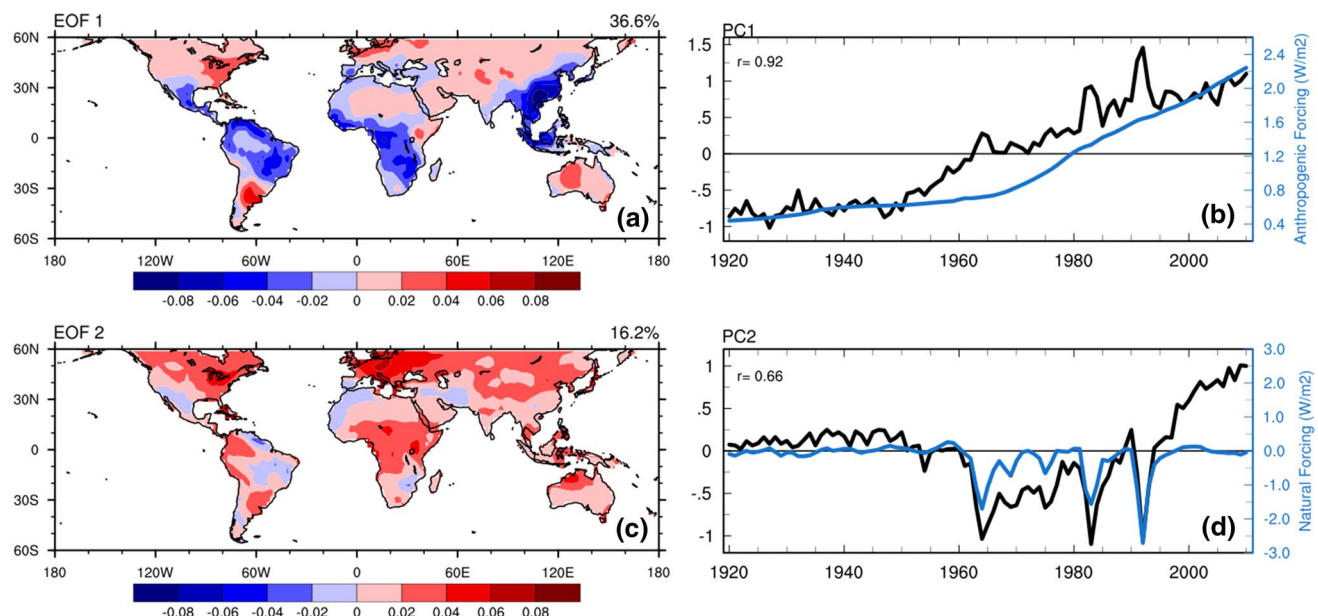
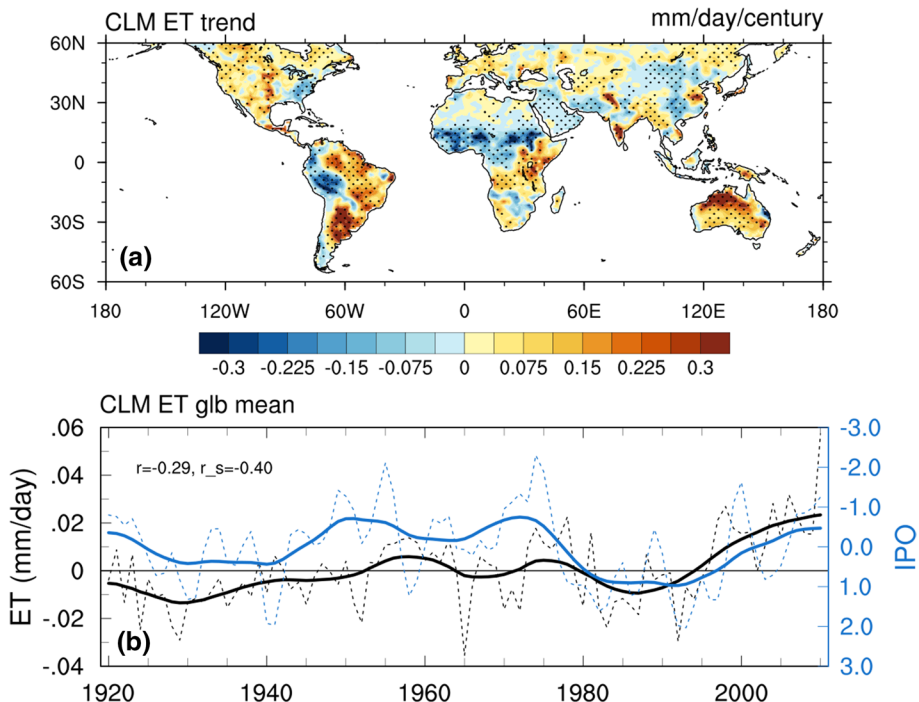


**Fig. 6** Spatial patterns (**a**, **c**) and the associated PCs (**b**, **d**, black curve) of the 1st (**a**, **b**) and 2nd (**c**, **d**) EOF mode of the CMIP5 multi-model ensemble mean ET from 1920–2010. The blue curves are anthropogenic (**b**) and natural (**d**) global-mean radiative forcing from

Fig. 8.18 of Myhre et al. (2013). The correlation between the PC and forcing series is shown in (**b**) and (**d**), and the explained percentage variance is shown on top of (**a**) and (**c**)

correlated ( $r = 0.92$ – $0.97$ ) with the anthropogenic forcing series (Fig. 7). In addition, the spatial pattern of the T for MCA1 (Fig. 7a, explains 96.2 % of the total T variance) exhibits warming over all land areas, which is the typical T response to GHG forcing (Collins et al. 2013), and similar

to the EOF1 of the CMIP5 model T from the all-forcing historical simulations (not shown). Thus, we consider MCA1 as the response to the anthropogenic forcing. On the other hand, the PCs for the second MCA mode (MCA2) (Fig. 8) show significant correlations ( $r = 0.55$ – $0.77$ ) with

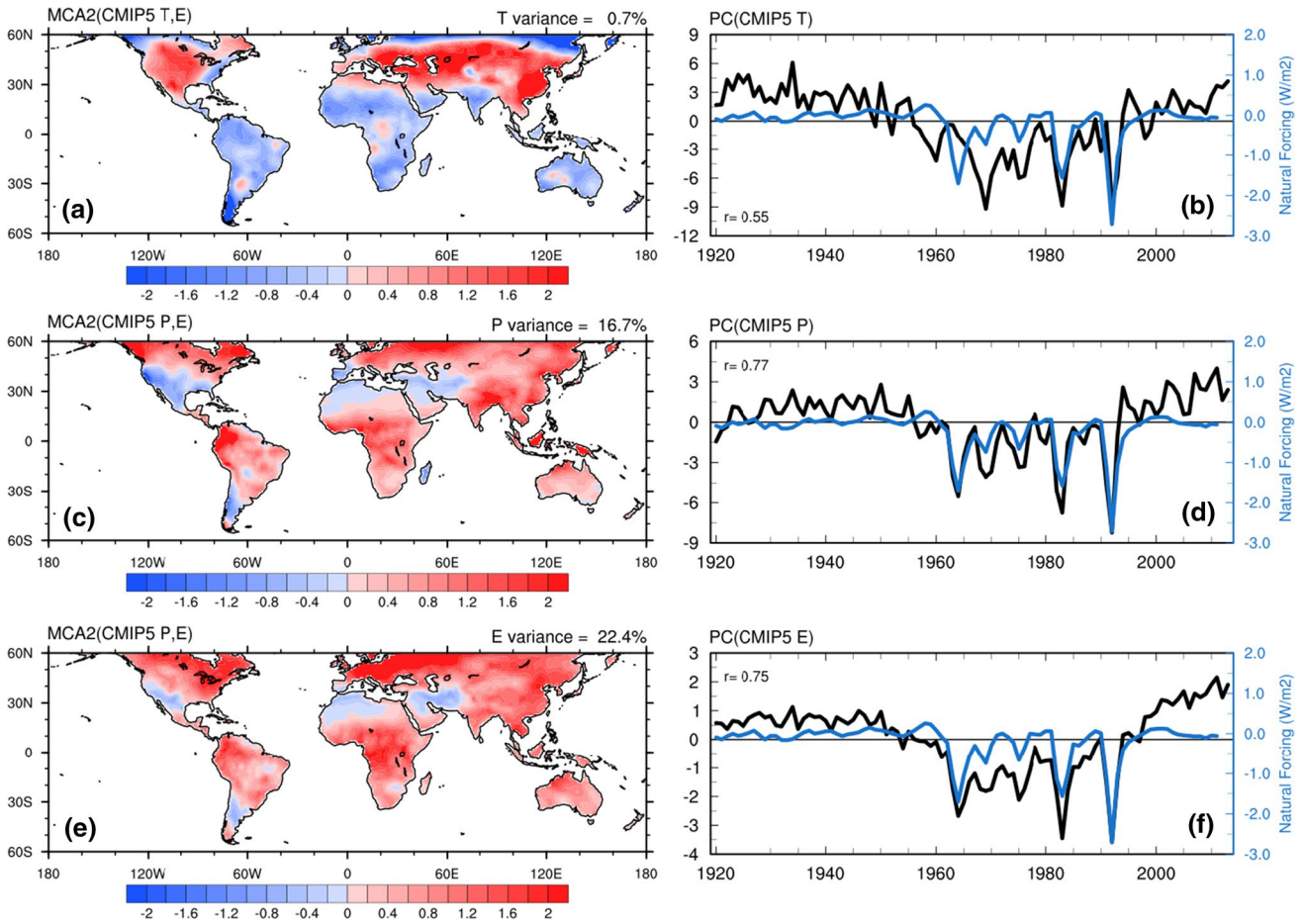


**Fig. 7** Spatial patterns (left) and the associated PCs (right, black line) of the 1st MCA mode for CMIP5 multi-model ensemble mean surface air temperature T (top row), precipitation P (middle row) and evaporation E (bottom row) derived from an MCA analysis of, respectively, the CMIP5 model T and ET, P and ET, and P and

ET from the all-forcing simulations (Taylor et al. 2012). The blue curve in the right panels is the anthropogenic radiative forcing from Fig. 8.18 of Myhre et al. (2013). The correlation between the PC and the forcing series is shown inside (b), (d), and (f). The explained percentage variance is shown on top of the (a), (c), and (e)

the natural forcing series, suggesting that this mode represents the response to the natural forcing.

The spatial patterns of the MCA1 for ET (Fig. 7e) are comparable to those for P (Fig. 7c, explains 29.8 % of the total P variance). This is also true for MCA2 (Fig. 8c, e). We also found broad spatial co-variations of ET and P for the CLM dataset (spatial pattern correlation = 0.71, figure not shown). Thus, the forced ET response closely follows the precipitation change patterns rather than those of T in the CMIP5 models. In contrast to T, the model simulated responses of P and ET to the anthropogenic forcing show large spatial variations, with increases in Australia and most of Eurasia and North America, but decreases over most of South America, Southeast Asia and Southwest North America and much of eastern and north-central Africa, (Fig. 7c, e), similar to Fig. 6a.

Besides the upward trend, the PC series in Fig. 7b shows large drops around 1963, 1982 and 1991 that coincide with

the recent volcanic forcing shown in Fig. 8b. These short-term variations are likely due to the mixing of the effects of the anthropogenic and natural forcings due to their similar spatial patterns (i.e., either uniformly warming or cooling), which makes it difficult for the MCA (or EOF) method to completely separate them into two different modes.

The MCA2 accounts for only 0.7 % of the total variance for T that comes primarily from GHG-induced trend; but 16.7 and 22.4 % of the variance for P and ET as in MCA2 (P, ET), respectively (Fig. 8). The spatiotemporal characteristics of the 2nd ET MCA mode with T, denoted as MCA2 (T, ET) which explains 19.5 % of the total ET variance, are similar to MCA2 (P, ET). The relatively low correlation ( $r = 0.55$ ) between the PC of T for MCA2 and the natural forcing (Fig. 8b) is likely due to the fact that some of the effect of the natural forcing is included in the MCA1 for T (Fig. 7b). Due to the very low percentage variance explained, the MCA2 pattern for T (Fig. 8a) is not very

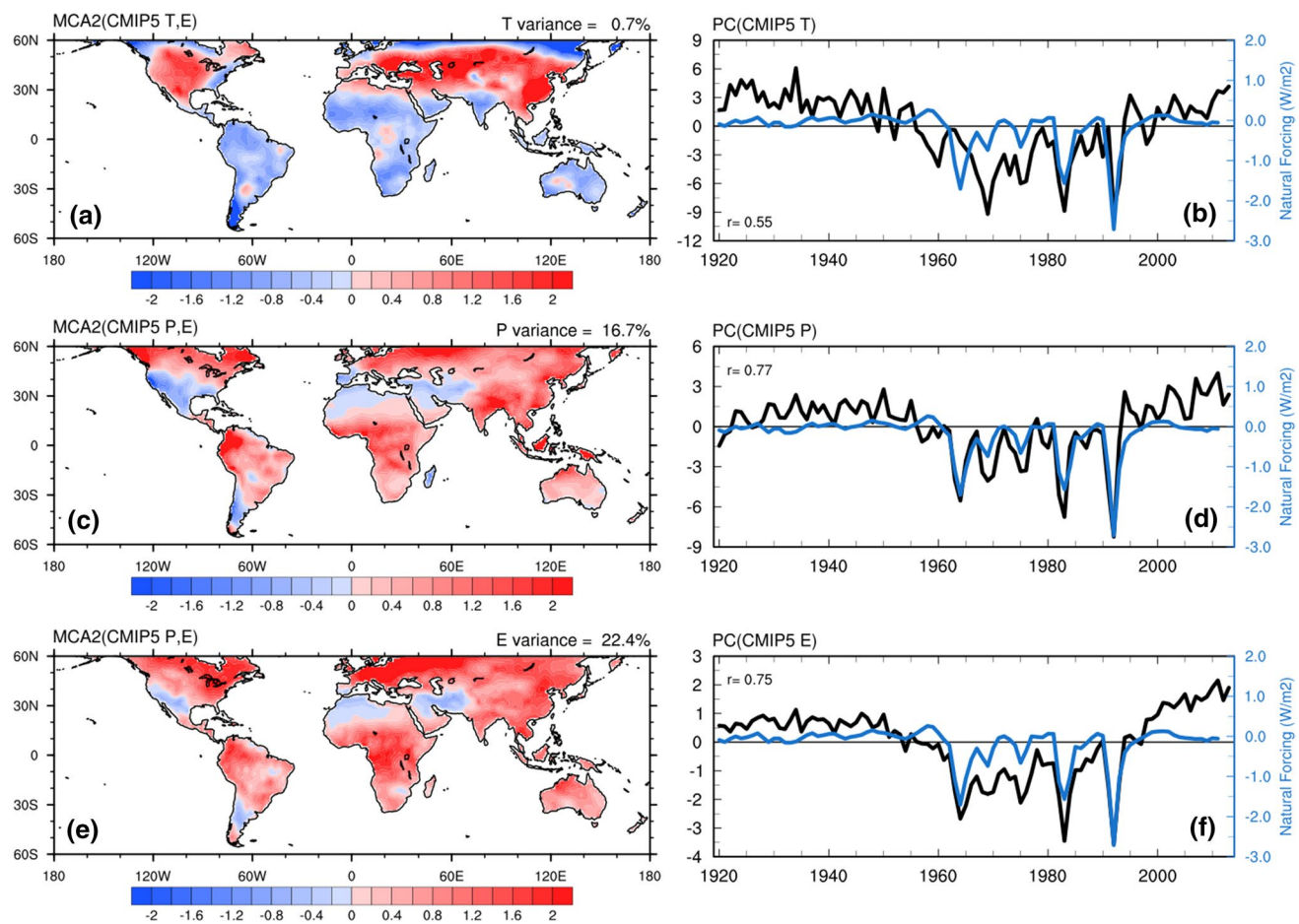


**Fig. 8** Same as Fig. 7 but for the 2nd MCA patterns and PCs. The blue line in the right panels is natural radiative forcing series from Fig. 8.18 of Myhre et al. (2013)

meaningful. The close overlap of the downward spikes of the PCs for P and ET and the natural forcing series in Fig. 8d, f suggests that the timing of the model-simulated responses for P and ET are realistic. This further suggests that the MCA2, especially for P and ET, represents the response to the natural forcing. Figure 8 shows that the recent volcanic eruptions in 1963, 1982 and 1991 caused decreases in P and ET over most land areas except Southwest North America, northern Africa and the Middle East. The MCA2 patterns for P and ET (Fig. 8c, e) differ considerably from those of MCA1 (Fig. 7c, e) that are induced by the anthropogenic forcing.

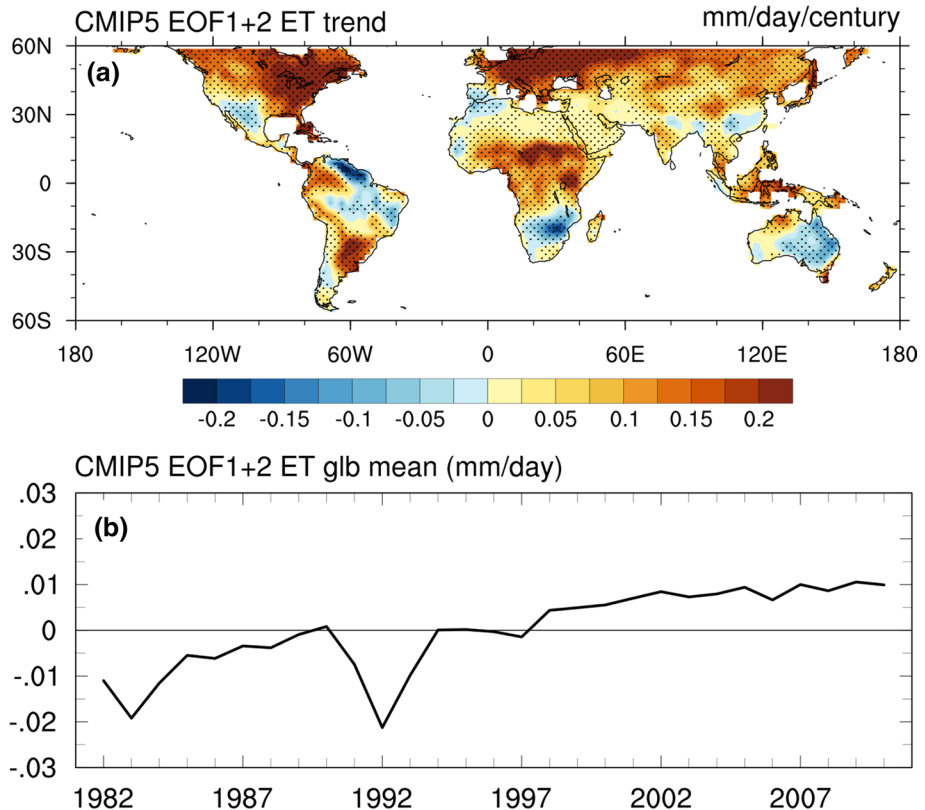
## 5 Attribution of ET to external forcings and natural climate variability

The trend patterns and the global-mean of the forced ET (based on the CMIP5 EOF1 and EOF2) re-scaled for the Miralles dataset are shown in Fig. 9. This forced

component (with slightly different re-scaling for the other two datasets as discussed in Sect. 2) was removed from the original ET time series from each of the three ET datasets to derive the unforced ET components at each grid box, whose trend maps are shown in Fig. 10. The magnitude of the forced ET differs slightly among the three datasets due to the re-scaling using the ET climatology of each dataset (see Sect. 2). The global-mean forced ET trends for the Miralles, Jung and CLM datasets are 0.07, 0.08 and 0.08 mm day<sup>-1</sup> century<sup>-1</sup>, respectively. Consequently, differences in the unforced ET trends are largely due to the differences in these ET datasets.

Figure 9 shows that the forced ET exhibits upward trends over most land areas especially Europe and eastern North America, except eastern and central Australia, southern Africa, southwest North America and a few other areas, where the forced ET actually shows decreasing trends (mainly due to decreasing precipitation). These patterns are broadly consistent with the projected ET changes by the end of 21st century (Collins et al. 2013; Zhao and Dai

**Fig. 9** **a** Map of the linear trend in the forced ET for the Miralles dataset from 1982 to 2010 reconstructed using the EOFs 1 and 2 of the CMIP5 multi-model ensemble mean ET, and **b** its global-mean time series. Stippling indicates the trend is statistically significant at the 10 % level. The trend map and time series for the Jung and CLM dataset (not shown) are very similar to this one. The trend in the global-mean forced ET is  $0.07 \text{ mm day}^{-1} \text{ century}^{-1}$



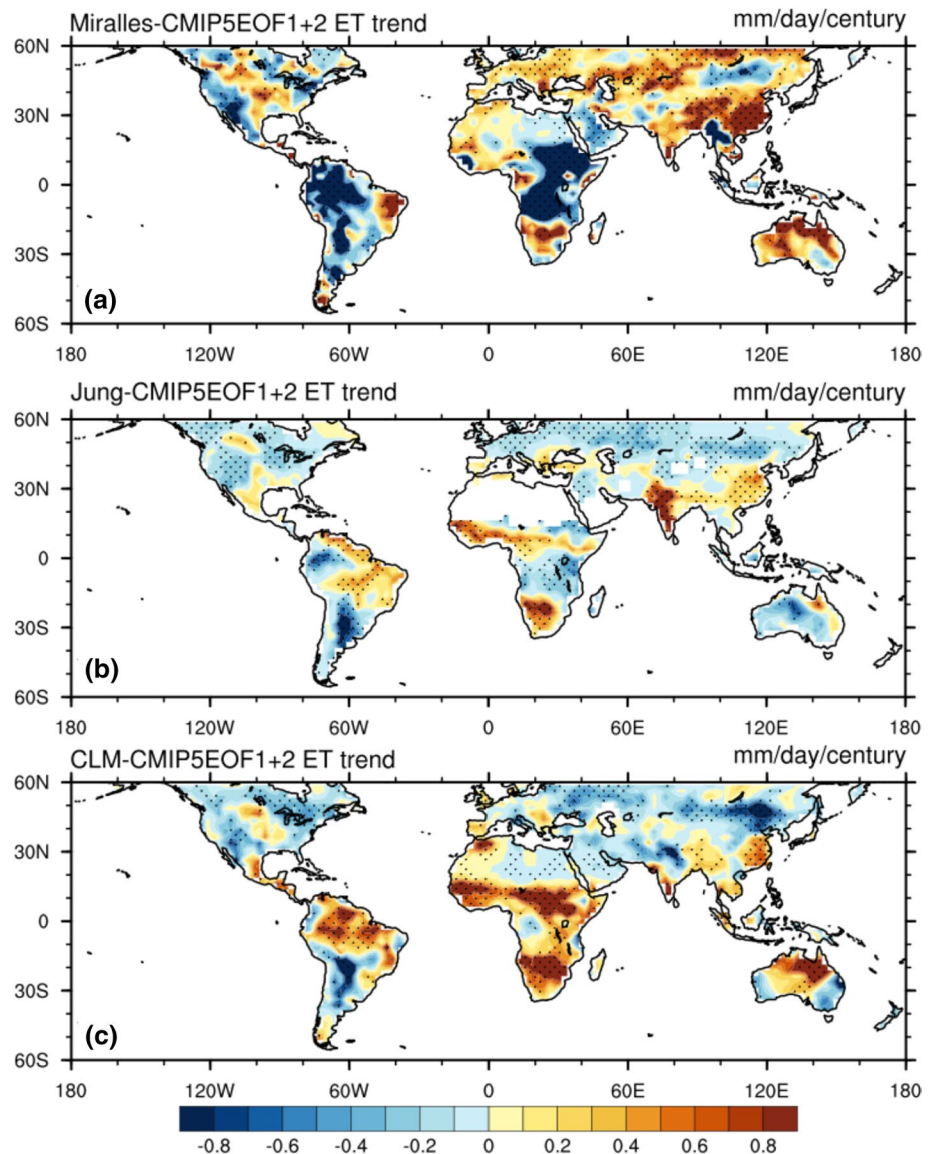
2015). The negative impact on ET by the 1991 Pinatubo and 1982 El Chichón volcanic eruptions is also evident in the forced ET (Fig. 9b). Compared with Fig. 2, it is clear that the forced ET cannot explain most of the regional ET changes during 1982–2010 in the three datasets. This suggests that natural climate variations, not the external forcings, are likely responsible for most of the regional change patterns in terrestrial ET during 1982–2010.

Figures 10 and 11 show that there are large disagreements in the apparent trends (likely due to decadal to multi-decadal variations) for the unforced ET among the three datasets in their regional patterns and global-mean series, although both the Jung and CLM data show decreasing ET during 1982–2010 over most Eurasia, North America and southern South America. In contrast, the Miralles ET shows large increases over most Eurasia and decreases over most South America and Africa (Fig. 10a). These trend patterns are expected from Fig. 2 because similar forced ET changes were subtracted from each of the ET estimates. Globally, the unforced ET from the CLM dataset exhibits an upward trend of 0.06 (significant at the 5 % level)  $\text{mm day}^{-1} \text{ century}^{-1}$ , comparable to the forced trend. However, no trend is detected for the Jung global-mean unforced ET, while the Miralles unforced ET shows a negative global trend of  $-0.07$  (significant at the 5 % level)  $\text{mm day}^{-1} \text{ century}^{-1}$ . The unforced ET trends are likely impacted negatively by recent Southern Hemisphere droughts during the period

from 2000 to 2008 (Jung et al. 2010). Clearly, the reliability of our estimates of the unforced ET trends shown in Figs. 10, 11 depends on the reliability of the forced ET trends derived from the CMIP5 multi-model ensemble mean.

Figure 11 compares the total and unforced global-mean ET with a Pacific Variability Index (PVI) that is defined as the 2nd PC of the 3-year averaged global SST fields, mostly from the Pacific (cf. Fig. 5b). The PVI contains more multi-year variations than the smoothed IPO index, which is the low-frequency component of the PVI. Thus, the co-variations shown in Fig. 11 reveals not only the multi-year ET vs. Pacific SSTs relation but also how Pacific SSTs and ET trends are related. We found that the correlation between the unforced ET and the PVI is statistically significant ( $r = -0.42$ ) only for the CLM dataset, although there are significant negative correlations between the actual ET and the PVI, mainly because of the apparent trends in these time series (Fig. 11). In other words, the GHGs and other external forcings have induced an upward trend in global-mean ET (Fig. 9) that could lead to significant correlations with the PVI during 1982–2010, as the IPO phase change around the late 1990s also induced an apparent trend in its index. The apparent trend in the PVI from 1982 to 2010 becomes part of the multi-decadal oscillations rather than a trend when examined from a longer time period, e.g., from 1920 to 2013 (Fig. 5b; Dai 2013; Dong and Dai 2015).

**Fig. 10** Maps of linear trend in unforced ET from 1982 to 2010 for the **a** Miralles, **b** Jung and **c** CLM dataset. Stippling indicates the trend is statistical significant at the 10 % level



Thus, one needs to be cautious in interpreting apparent trends in relatively short records.

Figure 12 shows the spatial distributions of the unforced ET vs. PVI correlation. Consistent among the three datasets, positive correlations are found over various regions, such as the western U.S., the Middle East and central and western Asia; while negative correlations are seen over Australia and southern Africa. Over many other regions such as central Africa and the Amazonia, however, there is no consensus on the sensitivity of unforced ET to the PVI among these datasets. These unforced ET-PVI correlation patterns are broadly consistent with both the ET-P and ET-T correlation patterns shown in Figs. 3, 4 and the T-PVI and P-PVI correlations shown in Fig. 13. For example, over the western U.S., the positive ET-PVI correlation (Fig. 12) is associated with strong positive P-PVI (Fig. 13b) and

P-ET correlations (Fig. 4). This suggests that western U.S. precipitation increases with the PVI, which in turn causes ET to increase with the PVI. Although ET is negatively correlated with T over much of the western U.S. (Fig. 3), PVI variations do not induce consistent T anomalies over this region (Fig. 13a), thus the ET-PVI correlation results mainly from tropical Pacific influence on P over this region. Over the Middle East, and central and western Asia, however, PVI-related changes in both T and P are significant (Fig. 13), with negative T and positive P anomalies for a positive PVI, and both T and P are correlated with ET over these regions (Figs. 3, 4, negative ET-T and positive ET-P correlation). Thus, the PVI-induced T and P anomalies would both lead to a positive ET-PVI correlation, as shown in Fig. 12. Over most Australia and southern African, negative ET-PVI correlations (Fig. 12) are associated with

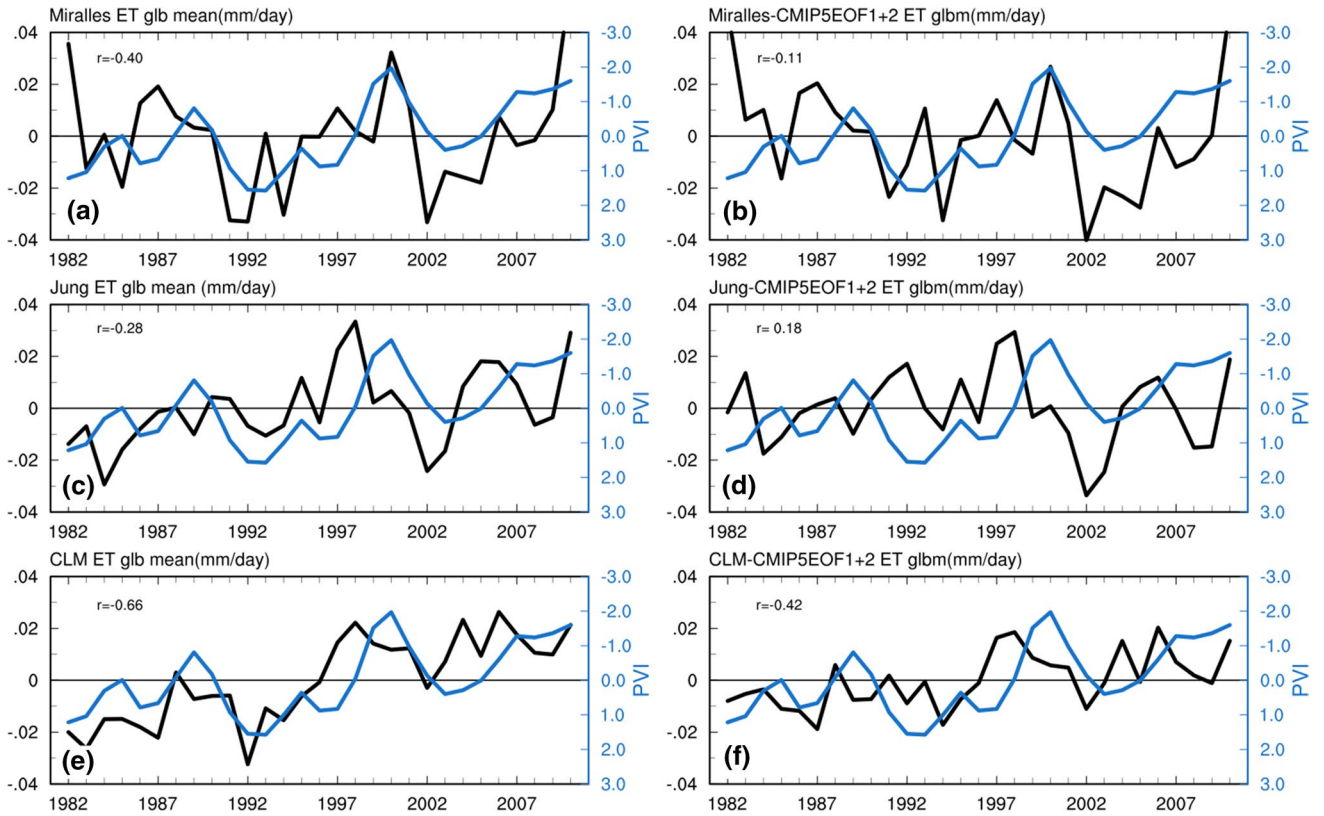


**Fig. 11** Global ( $60^{\circ}\text{S}$ – $60^{\circ}\text{N}$ ) averaged time series of the actual ET (left panels) and its unforced component (right panels) for the Miralles (top), Jung (middle) and CLM (bottom) dataset. The correlation coefficient between the ET time series (black line) and the PVI (blue line) is shown inside the panels. The trends in global-mean

actual (unforced) ET series for 1982–2010 are  $0.01$  ( $-0.07$ ),  $0.09$  ( $0.00$ ), and  $0.14$  ( $0.06$ )  $\text{mm day}^{-1} \text{century}^{-1}$ , respectively, from top to bottom. The correlation coefficient between the black lines in (b) and (d), (b) and (f), and (d) and (f) is, respectively,  $0.33$ ,  $0.15$ , and  $0.46$

positive T-PVI and negative P-PVI correlations (Fig. 13). Given the negative ET-T (Fig. 3) and strong positive ET-P (Fig. 4) correlations over these regions, the PVI-induced T and P anomalies would both induce negative ET anomalies for a positive PVI, consistent with the negative ET-PVI correlation shown in Fig. 12 for these two regions. Thus, the ET-PVI correlations shown in Fig. 12 are consistent with the T and P anomalies over land associated with Pacific SST variations caused by ENSO and IPO (Dai and Wigley 2000; Dong and Dai, 2015).

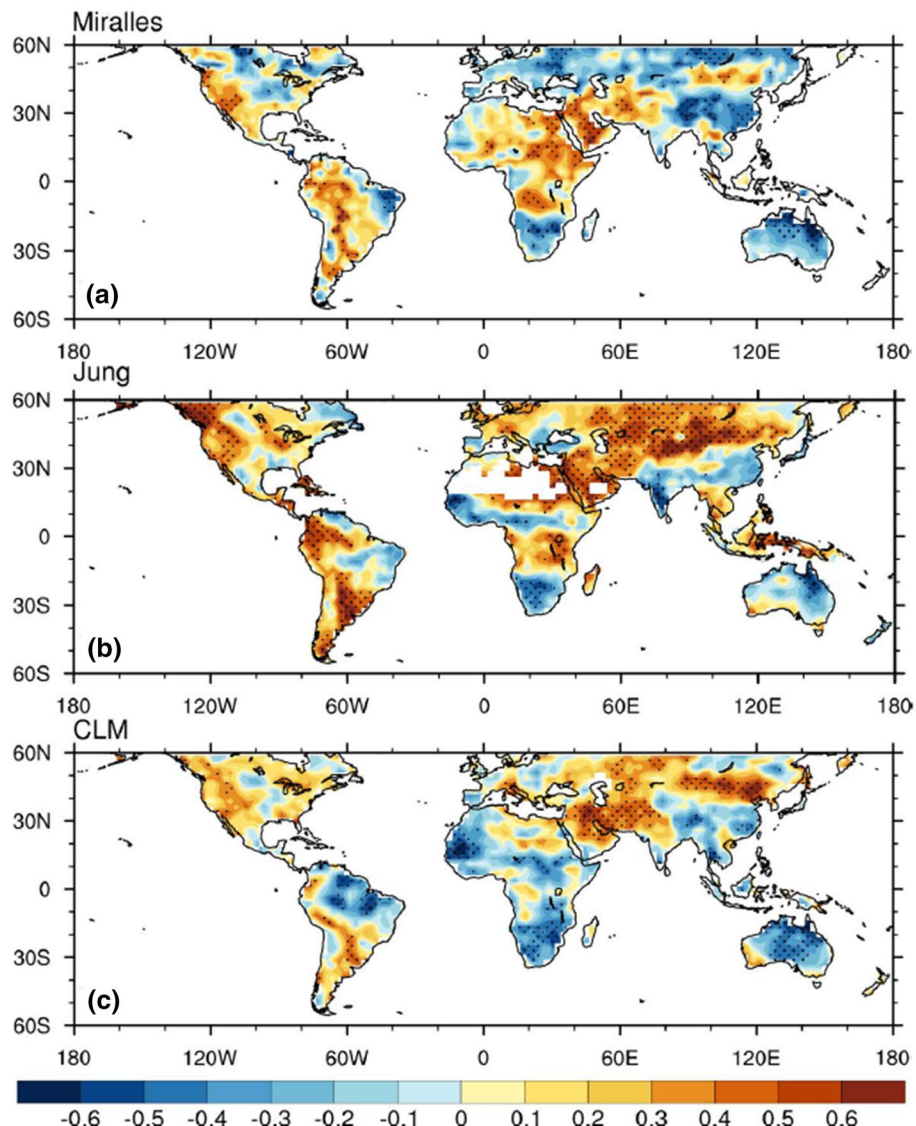
## 6 Summary and conclusions

We have investigated the causes of the recent (1982–2010) changes in global terrestrial ET, the characteristics of externally-forced ET changes, and the relative contributions of external forcing and natural variability using three different ET datasets and CMIP5 model historical simulations. Large discrepancies exist among these ET products in terms of interannual variability and trends at both regional and global scales. Significant upward

trends in global-mean ET are detected from 1982 to 2010 in the CLM ( $0.14 \text{ mm day}^{-1} \text{century}^{-1}$ ) and Jung ET ( $0.09 \text{ mm day}^{-1} \text{century}^{-1}$ ) but not in the Miralles dataset. Regionally, significant increases in ET are seen in all the three data sets over Europe, Southeast and high latitude Asia and southern Africa; while the Southwest U.S. and southern South America show downward ET trends during 1982–2010. However, different ET trends are seen over the Amazonia, the eastern U.S., the Sahel, eastern Africa, the maritime continent and Australia among these datasets. In particular, the Miralles ET shows considerably larger regional trends than the other two datasets. Although we were unable to provide an error bar for the ET trend from each of the datasets, the discrepancies among them suggest that there exist large uncertainties in the current estimates of ET over global land for the recent decades.

The ET vs. T and ET vs. P relationships also differ substantially among the three ET datasets, which reflects their distinct internal algorithms in generating these datasets. The Jung ET shows strong positive correlations with T over most northern mid- to high-latitudes, where the ET-T correlation is weaker for the Miralles and CLM ET. Both

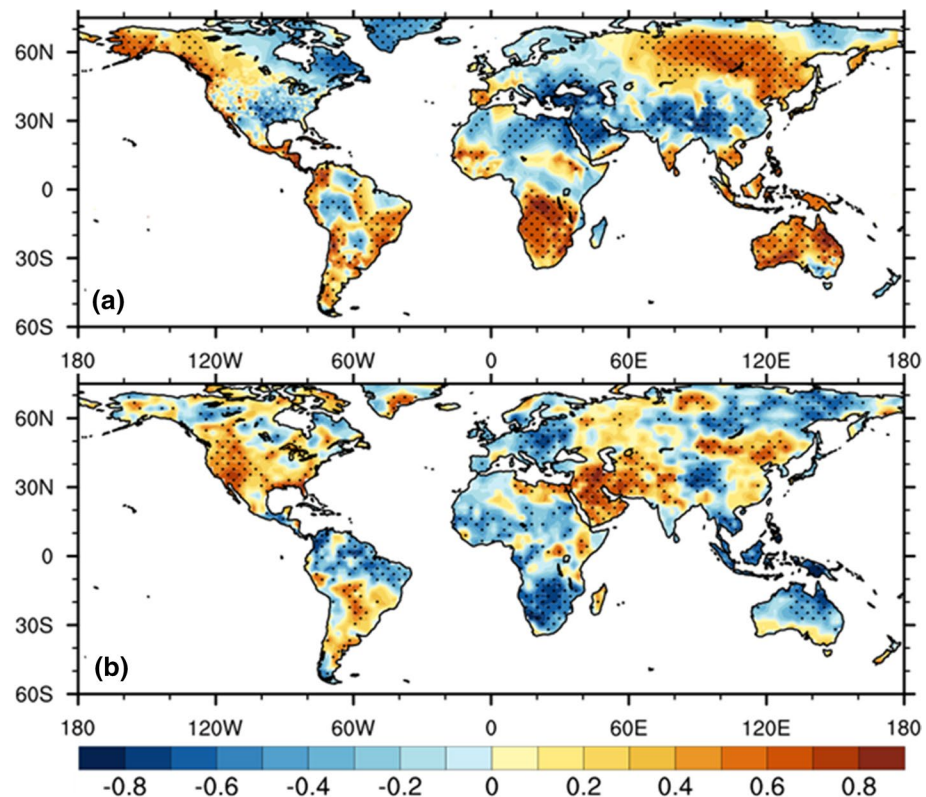
**Fig. 12** Maps of the correlation between the unforced ET and PVI for the **a** Miralles, **b** Jung and **c** CLM dataset from 1982 to 2010. Stippling indicates the correlation is statistical significant at the 10 % level



the Jung and CLM datasets show positive ET-T correlations over humid tropical Africa and South America and the maritime continent, while the Miralles ET shows generally negative correlations with T over these regions. All the three ET datasets show negative correlations with T over Australia, Southwest North America, southern Africa, the Middle East and other dry areas, which is expected since ET over arid and semi-arid land areas is water-limited and drier conditions reduce ET and thus lead to warmer T in these regions. These ET-T relationships imply that warming-induced increases in evaporative demand during recent decades over northern mid- and high-latitudes had larger impacts on the Jung ET than on the Miralles and CLM ET. The ET-T correlations are consistent with previous findings that T is an important controlling factor on ET over most parts of the northern mid- and high-latitudes (e.g., Mintz and Walker 1993; Nemani et al. 2003; Pan et al. 2015).

The ET-P correlations are generally positive over most land areas, especially over dry areas (e.g., Australia, the western U.S., southern Africa, western and central Asia) and for the CLM dataset. Together with the ET-T relation, it suggests that water supply is the limiting factor for ET over tropical and subtropical land areas. Such moisture control on ET over global dry lands is supported by many previous studies (e.g., Mintz and Walker 1993; Nemani et al. 2003; Pan et al. 2015). It also suggests that changes in precipitation from internal climate variability can have a strong influence on ET variability and decadal-multidecadal trends. Global-mean ET is found to be highly correlated with global-mean P and T for the CLM dataset partly due to their concurring trends, while the global-mean ET from the Jung dataset shows stronger correlation with T than with P. The global-mean ET from the Miralles dataset shows a weak trend and does not correlate well

**Fig. 13** Maps of the correlation between **a** CRU temperature and PVI and **b** GPCC precipitation and PVI from 1982 to 2010. Stippling indicates the correlation is statistical significant at the 10 % level. See text for the definition of the PVI



with either temperature or precipitation. We realize that in nature ET is also affected by changes in surface solar and longwave radiation, wind speed, and humidity, as well as other non-climatic factors such as CO<sub>2</sub> levels and land cover changes, although their roles are secondary compared to climatic constraints during recent decades (Mao et al. 2015; Pan et al. 2015). Nevertheless, the ET-T and ET-P correlations provide a measure of the relative importance of the energy control (through T) and water limitation (through P) over different regions among the three ET products.

Analyses of the CMIP5 multi-model ensemble mean ET, along with the model T and P data, suggest that the ET change patterns follow more closely with those of P rather than T. This is also true for the CLM ET dataset. In other words, the terrestrial water supply is the limiting factor for ET change over most land areas in the CMIP5 models and the CLM dataset. The GHGs and anthropogenic aerosols produce an upward trend in global-mean ET, with increases seen over most Eurasia (except Southeast Asia), North America (except its Southwest) and Australia but decreases over Central America and most South America, central to southern Africa, and Southeast Asia. The natural (volcanic + solar) forcing induces large multi-year to decadal variations in global ET since the 1950s, with large ET decreases over most land areas in the years following the volcanic eruptions in 1963, 1982 and 1991.

Similar to the original ET, we observed large discrepancies in the unforced ET component among the three datasets, although the reliability of the unforced ET trends depends on the reliability of the forced ET changes simulated by the CMIP5 models. There exists little correlation of the variations in the global-mean unforced ET during 1982–2010 among the three datasets, with a weak positive trend in the CLM unforced ET, a weak downward trend in the Miralles unforced ET and no trend in the Jung unforced ET. The change patterns of the unforced ET are broadly comparable to those in the original ET. This indicates that regional ET changes are mostly due to natural variability rather than the external forcing, even though the forced ET accounts for most of the global-mean trends seen in the Jung and CLM ET datasets.

Only the CLM global-mean ET shows significant negative correlation with the Pacific SSTs as represented by a Pacific variability index (PVI), and the upward trend of the CLM global-mean ET from 1982 to 2010 is concurrent with the downward PVI trend that is actually part of the IPO. Regionally, significant positive correlations of ET with PVI are seen over the western U.S., the Middle East and central and western Asia, while negative correlations are found over the eastern Australia and southern Africa among all the three ET datasets.

It's worth noting that the recent upward ET trend since the 1980s is the most prominent multi-decadal ET trend

among any other period of 30 years over the course of the twentieth century, according to the CLM ET dataset and the CMIP5 model simulations. Furthermore, this recent trend coincides with the recent IPO phase change that also induces an apparent trend in ET that can be mixed up with the GHG-induced changes. Simple regression or correlation analyses cannot separate these two concurring trends resulting from GHG forcing and the IPO phase change. Here, we relied on the CMIP5 model simulations to first estimate the externally forced ET changes. This allowed us to separate the forced and unforced changes, although the model-simulated ET changes likely contain uncertainties. Our results emphasize the importance of the internal climate variability (including the IPO) for terrestrial ET, especially on regional scales; although the externally forced ET is important for global-mean changes during recent decades.

**Acknowledgments** We thank Dr. Diego Miralles for kindly providing the Miralles ET dataset. We acknowledge the World Climate Research Programme's Working Group on Coupled Modelling, which is responsible for CMIP, and thank the international modeling groups and the Program for Climate Model Diagnosis and Intercomparison (PCMDI) for producing and making the CMIP5 data available. This work was supported by the U.S. National Science Foundation (Grant #AGS-1353740), the U.S. Department of Energy's Office of Science (Award #DE-SC0012602), and the U.S. National Oceanic and Atmospheric Administration (Award #NA15OAR4310086).

## References

- Angell JK (1993) Comparison of stratospheric warming following Agung, El Chichen and Pinatubo volcanic eruptions. *Geophys Res Lett* 20:715–718
- Bretherton CS, Smith C, Wallace JM (1992) An intercomparison of methods for finding coupled patterns in climate data. *J Clim* 5:541–560
- Collins M, Knutti R, et al. (2013) Long-term climate change: projections, commitments and irreversibility. In: Climate Change 2013: The physical science basis. Contribution of Working Group I to the Fifth Assessment Report of the Intergovernmental Panel on Climate Change [Stocker TF, Qin D, et al. (eds.)]. Cambridge University Press, Cambridge, United Kingdom and New York, NY, USA, pp. 1029–1136
- Dai A (2013) The influence of the inter-decadal Pacific oscillation on US precipitation during 1923–2010. *Clim Dyn* 41(3–4):633–646. doi:[10.1007/S00382-012-1446-5](https://doi.org/10.1007/S00382-012-1446-5)
- Dai A (2016) Historical and future changes in streamflow and continental runoff: A review. AGU Monograph entitled “Terrestrial Water Cycle and Climate Change: Natural and Human-induced Impacts”, Q. Tang et al. (eds.), in press.
- Dai A, Wigley TML (2000) Global patterns of ENSO-induced precipitation. *Geophys Res Lett* 27(9):1283–1286. doi:[10.1029/1999GL011140](https://doi.org/10.1029/1999GL011140)
- Dai A, Fung IY, Del Genio AD (1997) Surface observed global land precipitation variations during 1900–1988. *J Clim* 10:2943–2962
- Dai A, Qian T, Trenberth KE, Milliman JD (2009) Changes in continental freshwater discharge from 1949–2004. *J Clim* 22:2773–2791
- Dingman SL (2015) Physical hydrology, 3rd edn. Waveland Press, Long Grove, p 643
- Dong B, Dai A (2015) The Influence of the Interdecadal Pacific Oscillation on Temperature and Precipitation over the Globe. *Clim Dyn*:1–15. doi:[10.1007/s00382-015-2500-x](https://doi.org/10.1007/s00382-015-2500-x)
- Feng S, Fu Q (2013) Expansion of global drylands under warming climate. *Atmos Chem Phys* 13:10081–10094
- García-García D, Ummenhofer CC (2015) Multidecadal variability of the continental precipitation annual amplitude driven by AMO and ENSO. *Geophys Res Lett* 42(2):526–535
- Gu G, Adler RF (2013) Interdecadal variability/long-term changes in global precipitation patterns during the past three decades: global warming and/or pacific decadal variability? *Clim Dyn* 39:3009–3022. doi:[10.1007/s00382-012-1443-8](https://doi.org/10.1007/s00382-012-1443-8)
- Gu G, Adler RF (2015) Spatial patterns of global precipitation change and variability during 1901–2010. *J Clim* 28:4431–4453. doi:[10.1175/JCLI-D-14-00201.1](https://doi.org/10.1175/JCLI-D-14-00201.1)
- Gu G, Adler RF, Huffman GJ (2016) Long-term changes/trends in surface temperature and precipitation during the satellite era (1979–2012). *Clim Dyn* 46:1091–1105. doi:[10.1007/s00382-015-2634-x](https://doi.org/10.1007/s00382-015-2634-x)
- Harris I, Jones PD, Osborn TJ, Lister DH (2014) Updated high-resolution grids of monthly climatic observations – the CRU TS3.10 Dataset. *Int J Climatol* 34:623–642. doi:[10.1002/joc.3711](https://doi.org/10.1002/joc.3711)
- Hu Q, Feng S (2012) AMO- and ENSO-Driven Summertime Circulation and Precipitation Variations in North America. *J Climate* 25(19):6477–6495. doi:[10.1175/Jcli-D-11-00520.1](https://doi.org/10.1175/Jcli-D-11-00520.1)
- Jung M, Reichstein M, Ciais P, Seneviratne SI, Sheffield J, Goulden ML, Bonan G, Cescatti A, Chen JQ, de Jeu R, Dolman AJ, Eugster W, Gerten D, Gianelle D, Gobron N, Heinke J, Kimball J, Law BE, Montagnani L, Mu QZ, Mueller B, Oleson K, Papale D, Richardson AD, Roupsard O, Running S, Tomelleri E, Viovy N, Weber U, Williams C, Wood E, Zaehele S, Zhang K (2010) Recent decline in the global land evapotranspiration trend due to limited moisture supply. *Nature* 467(7318):951–954. doi:[10.1038/Nature09396](https://doi.org/10.1038/Nature09396)
- Liu ZY (2012) Dynamics of interdecadal climate variability: a historical perspective. *J Clim* 25:1963–1995
- Mantua NJ, Hare SR, Zhang Y, Wallace JM, Francis RC (1997) A Pacific interdecadal climate oscillation with impacts on salmon production. *Bull Am Meteorol Soc* 78:1069–1079. doi:[10.1175/1520-0477\(1997\)078<1069:APICOW>2.0.CO;2](https://doi.org/10.1175/1520-0477(1997)078<1069:APICOW>2.0.CO;2)
- Mao J, Fu W, Shi X, Ricciuto DM, Fisher JB, Dickinson RE, Wei Y, Shem W, Piao S, Wang K, Schwalm CR (2015) Disentangling climatic and anthropogenic controls on global terrestrial evapotranspiration trends. *Environmental Research Letters* 10(9):094008
- Mintz Y, Walker GK (1993) Global fields of soil moisture and land surface evapotranspiration derived from observed precipitation and surface air temperature. *J Appl Meteorol* 32(8):1305–1334
- Miralles DG, van den Berg MJ, Gash JH, Parinussa RM, de Jeu RAM, Beck HE, Holmes TRH, Jimenez C, Verhoest NEC, Dorigo WA, Teuling AJ, Dolman AJ (2014) El Nino-La Nina cycle and recent trends in continental evaporation. *Nat Clim Change* 4(2):122–126. doi:[10.1038/Nclimate2068](https://doi.org/10.1038/Nclimate2068)
- Monahan AH, Fyfe JC, Ambaum MHP, Stephenson D, North GR (2009) Empirical orthogonal functions: The medium is the message. *J. Climate* 22:6501–6514
- Myhre G, Shindell D, Bréon FM, Collins W, Fuglestvedt J, Huang J, Zhang H (2013) Anthropogenic and Natural Radiative Forcing. In: Climate Change 2013: The Physical Science Basis. Contribution of Working Group I to the Fifth Assessment Report of the Intergovernmental Panel on Climate Change [Stocker TF, Qin D, Plattner G-K, Tignor M, Allen SK, Boschung J, Nauels A, Xia Y, Bex V, Midgley PM (eds.)]. Cambridge University Press, Cambridge, United Kingdom and New York, NY, USA, pp. 659–740.

- Nemani RR, Keeling CD, Hashimoto H, Jolly WM, Piper SC, Tucker CJ, Myneni RB, Running SW (2003) Climate-driven increases in global terrestrial net primary production from 1982 to 1999. *Science* 300(5625):1560–1563
- Oleson K, Lawrence D, Bonan G, Drewniak B, Huang M, Koven C, Levis S, Li F, Riley W, Subin Z (2013) Technical description of version 4.5 of the Community Land Model (CLM). Ncar Tech. Note NCAR/TN-503 + STR. National Center for Atmospheric Research, Boulder, CO, 422 pp. doi: [10.5065/D6RR1W7M](https://doi.org/10.5065/D6RR1W7M).
- Pan S, Tian H, Dangal SR, Yang Q, Yang J, Lu C, Tao B, Ren W, Ouyang Z (2015) Responses of global terrestrial evapotranspiration to climate change and increasing atmospheric CO<sub>2</sub> in the 21st century. *Earth's Future* 3(1):15–35
- Piao SL, Ito A, Li SG, Huang Y, Ciais P, Wang XH, Peng SS, Nan HJ, Zhao C, Ahlstrom A, Andres RJ, Chevallier F, Fang JY, Hartmann J, Huntingford C, Jeong S, Levis S, Levy PE, Li JS, Lomas MR, Mao JF, Mayorga E, Mohammat A, Muraoka H, Peng CH, Peylin P, Poulter B, Shen ZH, Shi X, Sitch S, Tao S, Tian HQ, Wu XP, Xu M, Yu GR, Viovy N, Zaehle S, Zeng N, Zhu B (2012) The carbon budget of terrestrial ecosystems in East Asia over the last two decades. *Biogeosciences* 9(9):3571–3586. doi: [10.5194/bg-9-3571-2012](https://doi.org/10.5194/bg-9-3571-2012)
- Ropelewski CF, Halpert MS (1987) Global and regional scale precipitation patterns associated with the El Niño/Southern Oscillation. *Mon Weather Rev* 115(8):1606–1626
- Ropelewski CF, Halpert MS (1989) Precipitation patterns associated with the high index phase of the Southern Oscillation. *J Clim* 2(3):268–284
- Scheff J, Frierson DMW (2014) Scaling potential evapotranspiration with greenhouse warming. *J Clim* 27:1539–1558. doi: [10.1175/JCLI-D-13-00233.1](https://doi.org/10.1175/JCLI-D-13-00233.1)
- Schneider U, Fuchs T, Meyer-Christoffer A, Rudolf B (2008) Global precipitation analysis products of the GPCC. Global Precipitation Climatology Centre (GPCC), Deutscher Wetterdienst: Offenbach, Germany. DWD, Internet Publikation 112. Available at <http://gpcc.dwd.de>.
- Seo KW, Waliser DE, Tian B, Kim BM, Park SC, Cocke S, Sohn BJ, Ishii M (2012) Evidence of the recent decade Change in Global Fresh Water Discharge and Evapotranspiration Revealed by Reanalysis and Satellite Observations. *Asia-Pac J Atmos Sci* 48(2):153–158. doi: [10.1007/S13143-012-0015-5](https://doi.org/10.1007/S13143-012-0015-5)
- Taylor KE, Stouffer RJ, Meehl GA (2012) An overview of CMIP5 and the experiment design. *Bull Am Meteorol Soc* 93:485–498
- Wang K, Dickinson RE (2012) A review of global terrestrial evapotranspiration: Observation, modeling, climatology, and climatic variability. *Rev Geophys* 50, RG2005, doi: [10.1029/2011RG000373](https://doi.org/10.1029/2011RG000373).
- Wild M, Grieser J, Schär C (2008) Combined surface solar brightening and increasing greenhouse effect support recent intensification of the global land-based hydrological cycle. *Geophys Res Lett* 35:L17706. doi: [10.1029/2008GL034842](https://doi.org/10.1029/2008GL034842)
- Yan H, Yu Q, Zhu ZC, Myneni RB, Yan HM, Wang SQ, Shugart HH (2013) Diagnostic analysis of interannual variation of global land evapotranspiration over 1982–2011: Assessing the impact of ENSO. *J Geophys Res-Atmos* 118(16):8969–8983. doi: [10.1002/jgrd.50693](https://doi.org/10.1002/jgrd.50693)
- Zeng ZZ, Piao SL, Lin X, Yin GD, Peng SS, Ciais P, Myneni RB (2012) Global evapotranspiration over the past three decades: estimation based on the water balance equation combined with empirical models. *Environ Res Lett* 7(1). doi: [Artn 014026](https://doi.org/10.1088/1748-9326/7/1/014026).
- Zhang Y, Wallace JM, Battisti DS (1997) ENSO-like interdecadal variability: 1900–1993. *J Climate* 10(5):1004–1020. doi: [10.1175/1520-0442](https://doi.org/10.1175/1520-0442)
- Zhao T, Dai A (2015) The magnitude and causes of global drought changes in the 21<sup>st</sup> century under a low-moderate emissions scenario. *J. Climate* 28:4490–4512